

The origin of the color of pearls in iridescence from nano-composite structures of the nacre

MICHAEL R. SNOW,^{1,*} ALLAN PRING,¹ PETER SELF,² DUSAN LOSIC,³ AND JOE SHAPTER³

¹South Australian Museum, North Terrace, Adelaide, South Australia 5000, Australia

²Adelaide Microscopy, University of Adelaide, North Terrace, South Australia 5000, Australia

³School of Physical Sciences, The Flinders University of South Australia, GPO Box 2100, Adelaide, South Australia 5001

ABSTRACT

The origin of the variety of body colors exhibited by South Sea Pearls is in part due to a newly recognized structure of the nacre, the edge-band structure, which gives rise to interference colors characteristic of its width. With the pearl oyster, *Pinctada maxima*, the colors include a range of silver tones, creams, yellows, and gold in various degrees of color saturation. We establish here that the primary body color of *P. maxima* pearls arises from the interference of light within the binding regions of the aragonite tiles. The tile faces terminate in a fissured nano-composite structure containing organic matrix within the margin of the aragonite tiles. This edge-band structure gives rise to an optical film formed of organic matrix in aragonite. The TEM images show that the edge-band structure width increases progressively from 74(4) nm in a silver pearl, to 80(4) nm in a cream pearl, and to 90(4) nm in a gold pearl. These colors are the first-order Newton's colors, which, when mixed with the specular reflection of the nacre and modified by any pigmentation present, give rise to the body color of pearls. The non-metallic whiter pearls more commonly seen can be accounted for by disorder of this structure leading to unsaturation of the color.

INTRODUCTION

The pearl oysters are members of the family *Pteriacea* and have shells composed of an outer fibrous periostracum covering a calcitic prismatic layer. The inside of the shell is composed of two nacreous layers: an outer layer, which is attached to the calcitic prismatic layer, and an inner layer that lines the inside of the shell and comes in contact with the oyster. The outer nacreous layer projects beyond the inner layer to form a lip at the edge of the shell (Taylor et al. 1973). In *P. maxima*, the color of this lip gives rise to the common names “silver” or “gold” lip oysters and, in *P. margaritifera*, to “black” lip oysters. Such colors are seen in the pearls formed by these oysters, which are known commercially as South Sea Pearls.

Cultured pearls consist of nacre, a microstructure of aragonite crystals (tiles), approximately $10 \times 7 \times 0.4 \mu\text{m}$, held together by an organic matrix, overlaid on a shell bead nucleus formed usually from pigtoe mussel shell. Figure 1 shows the nacre in cross-section. A pearl is essentially the outer nacreous layer of the mollusc formed into a spherical shape. A pearl is cultured by inserting a selected piece of mantle tissue from a sacrificial oyster, together with a bead nucleus into the gonad of the partly opened oyster. Over time a tissue pearl sac is developed around the bead and successive layers of nacre are laid down (Webster and Anderson 1983; Landman et al. 2001). The lip colors are used as a guide in the selection of the sacrificial mantle. The expectation in the pearl industry is that the color of the lip of the donor oyster will be reproduced in the pearls.

The iridescent colors of South Sea Pearls and their shells have been ascribed to interference and/or diffraction effects (Webster and Anderson 1983). The rainbow-like diffraction colors arise

from surface repetition of the nacre layers (growth lines) and are known by gemmologists as the “orient”. These surface diffraction effects are well established to account for the multicolored iridescences seen in some shells (Raman 1934; Webster and Anderson 1983; Liu et al. 1999). Generally, the effect is more strongly evident on the inside of the shell than on a pearl, and the diffraction effect can still be seen on the wax impressions of the shells. Not all iridescence, however, arises from surface regularities (see Discussion). The strength of the effect is related to the density of the growth lines (Liu et al. 2003). The observed color and intensity of the orient can add considerable value to pearls, and pearl farmers have been able to alter the orient by changing the environmental conditions of the growth (Arrow 1999, personal communication).

Pearls exhibit a wide variety of body colors, the origin of which has not been clearly established (Webster and Anderson 1983; Newman 1999; Landman et al. 2001). With the pearl oyster, *P. maxima*, the colors include whites, a range of silver tones, creams, yellows, and gold. The color of the silver and yellow pearls can be strongly metallic in appearance. There is substantial evidence that the pearl nacre color is related to the nature of the mantle cells that were used to supply the graft implant (Taylor 2002). The existence of two-tone pearls, often silver and cream with a transition zone, arises from the differing rows of color cells on the mantle tissue. Commercial pearls, however, from this species and the Japanese akoya pearl oyster *P. fucata martensi* are often white or off white to cream and do not exhibit strong metallic luster. In *P. margaritifera*, the black pearl oyster, deep black and dark silvery body tones with a green sheen due to diffraction from the surface are highly prized. The major cause of body color variation in these pearls has been ascribed to pigments (Elen 2002).

We initially considered that the origins of body color might

* E-mail: snow.mike@saugov.sa.gov.au

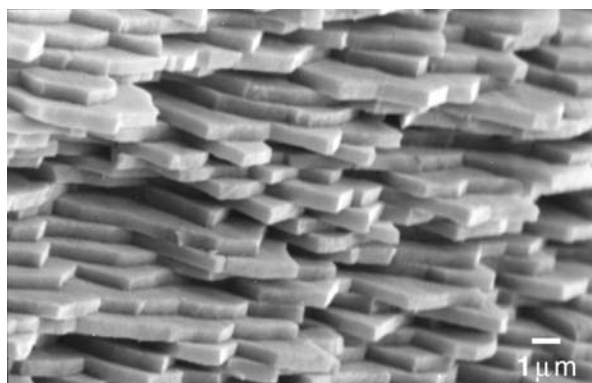


FIGURE 1. SEM image of the cross-section of a broken pearl showing the aragonite crystal tiles. The aragonite *c* axis of the tiles projects vertically from the nacre, but the orientation of the *a* and *b* axes is not constrained (Chateigner et al. 2000).

lie either in pigmentation of the organic matrix between the aragonite tiles or in optical interference within the tiles of the nacre. The organic materials of mollusc shells decalcified with dilute acid were first called conchiolin by Frémy (1855). The term can include the outer periostracum and dark layers within the shell. In this paper, the term organic matrix is used specifically for the organic material binding the aragonite tiles; the term “conchiolin membrane” has also been used for this material (Iwata 1975). Recently, it has been shown to consist mainly of β -chitin, with lesser amounts of a glycoprotein (Levi-Kalisman et al. 2001). In many cases, shells also contain separate conchiolin layers, which are primarily dark-colored organic material and these can strongly influence the body color. In pearls with thin nacre, this organic matter can darken the body tone; so-called blue pearls, pearls of a leaded-grey color, are of this nature (Webster and Anderson 1983). Interference within the gap of organic matrix between the tiles has also been modeled to explain pearl color (Nagata et al. 1997).

Yellow pigment components have been reported in some pearls (Koizumui and Nonaha 1970), but significant trace metals as a source of color in *P. maxima* pearls has been rejected based on extensive trace-element analysis (Lambert 1998). The yellow color in these pearls has been suggested to be zoochrome absorbing in the blue region (Elen 2001), based on spectral analysis alone. Yellow colors can be induced by heat treatment (Elen 2001, 2002), but these pearls differ spectroscopically from the yellow untreated pearls.

MATERIALS AND METHODS

A selection of cultured *P. maxima* pearls, covering the full spectrum of body colors, was provided by Atlas Pacific Limited from pearl farms in Indonesia. These pearls were cut in half with a diamond saw and one half kept for color reference. The other half was broken and thin fracture fragments were embedded in epoxy resin and sectioned perpendicular to the thickness of the plates using a diamond knife. Careful note was taken of the orientation of the fragments so the growth direction could be determined. Thicknesses from 50 to 200 nm were cut with the microtome. These sections were floated on water and transferred onto Cu support grids that had been coated with thin carbon support films. Sections were examined using a 200-kV Philips CM200 electron microscope fitted with a standard side-entry goniometer ($\pm 60^\circ$), objective lens with $C_s = 2.00$ mm, and a W filament. SEM images were obtained on freshly broken pearl fragments that had been sputter coated with a thin layer of Au/Pt using Philips XL20 and XL30

scanning electron microscopes.

The TEM negatives were scanned with a high-resolution scanner (Epson 2450 Photo) and displayed and measured with Adobe Photoshop 6. The magnification of the TEM images was carefully calibrated using latex spheres of known size. Measurements were averaged to derive the values and standard deviations given in the text.

AFM images were obtained using a MultiMode microscope in conjunction with the Nanoscope IV system (Digital Instrument, Santa Barbara, CA). Both “E” and “J” scanners were used with lateral ranges of 10 and 125 nm. Imaging was carried out using tapping mode in air. Silicon cantilevers (DI, model TESP) that operate at the frequency of 300–400 kHz were used. Height and phase data were collected simultaneously at scan rates between 1 and 2 Hz. Pearl sections were polished using 0.25 μ m alumina paste in water until a very high quality finish was obtained, and sonicated in water solution followed by drying with a stream of nitrogen. Samples were probed in a minimum of 5 different spots, and images were collected with edge lengths of 50, 20, 10, 5, and 1 μ m.

RESULTS

A TEM micrograph of a cross-section of pearl nacre reveals the microstructure of the aragonite tiles and the organic matrix (Fig. 2). There are prominent fissured bands at the tile edges. Electron diffraction revealed that these fissured bands, which we call the edge-band structure, are crystallographically continuous with the rest of the aragonite tile. All the pearls studied show this microstructural feature, as does the shell lip (outer nacreous layer) and, to a lesser degree, the inner nacreous layers of the shell. It is known that the organic matrix controls the process of aragonite crystallization in shells (Weiner et al. 1983). Iwata (1975) found that an insoluble organic matrix surrounds the aragonite tiles and that a water soluble protein is incorporated into them (Weiner and Hood 1975), but evidence for this banding structure within the edges of the tiles has not been reported. Much of this previous work has been done on abalone nacre. We found that the Paua abalone, *Halatois iris*, indeed does not display this edge-band structure.

The extent of the edge structure in these pearls can be readily seen in the images of a very thin broken microtome section (Fig. 3). Here, the body of the aragonite tile has dropped out and only the remnant edge structure remains in places such as that shown expanded in Figure 3. The remnant edges are the same width as the edge bands observed in undamaged sections like those shown in Figure 2. This correlation supports the suggestion that the edge-band consists of a composite of aragonite and organic matrix.

Figure 4 shows an AFM image of the microstructure of a silver pearl viewed in the same direction as in Figure 2. The image shows that the edge-band organic matrix projects above the middle of the aragonite tiles by about 10 nm; the separations between the tiles in the same row are not now visible. The composite bands on adjacent tiles in the same row have been merged into a ridge in the image. As observed in the AFM images, the ratio of the width of these bands to that of the tiles is approximately 1 to 4, in accord with the 1 to 5 ratio seen in the TEM images, indicating that they are the same bands. Attempts to obtain quantitative widths from these AFM images were not satisfactory. What is seen is the convolution of the finite AFM tip with the surface; due to tip wear, the same experiments cannot be repeated on a series of differently colored pearls. It was found that the aragonite tiles in pearls show a wide variation in thickness, both within a single pearl and among pearls of the same color. The variation is from about 300 nm to 600 nm, with an average of

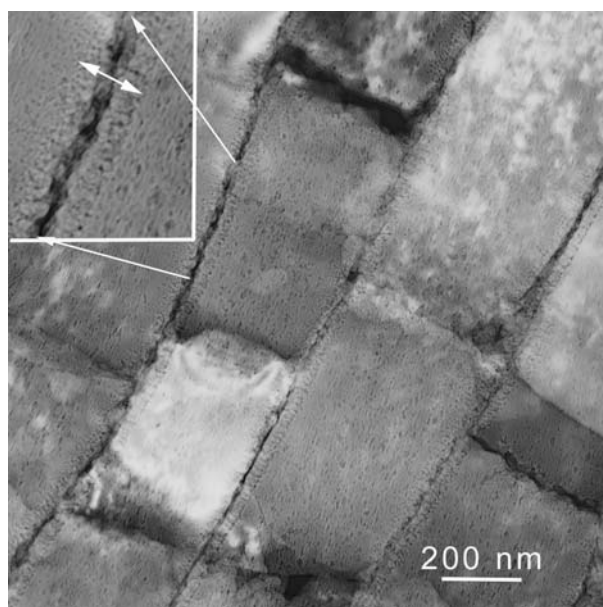


FIGURE 2. TEM micrograph of a silver pearl, sectioned perpendicular to the nacre tiles. The insert is enlarged by 2 \times in each direction to show the intra tile organic matrix forming the edge-band structure.

about 400 nm. The standard deviation of any group of measurements is very large, around 70 to 100 nm. Other *P. maxima* pearls studied, with differing colors, also show this wide variation in tile width. No correlation between tile thickness and pearl color could be established. The colored lips of *P. maxima* shells gave a very similar set of size ranges. The white inner nacreous layer of the shells was found to be less regular, consisting of aragonite tiles having irregular thickness and shape.

The TEM images (Fig. 2) show that the walls of the gap between the aragonite tiles are not smooth. Significant surface features also have been reported in gastropods as either mineral bridges (Schaffer et al. 1997; Addadi and Weiner 1997) and in *P. maxima* as lumpy nano asperities (Wang et al. 2001). The evidence we provide supports the notion of mineral bridges in this species, i.e., single aragonite crystals growing through the organic layer between the tiles so that adjacent tiles are crystallographically continuous. TEM images of demineralized specimens (Fig. 5) show regular pores of diameter 30(4) nm spaced between 80 and 120 nm apart in the residual strips of organic matrix from between the tiles (standard deviations given in parenthesis). The density of pores is 115(20) per μm^2 and they occupy 8% of the area. Plecypoda molluscs with pore sizes in the range 10 to 50 nm and occupying about 10% of the area have been reported (Iwata 1975). In the gastropod *Paua* (*H. iris*), the size of mineral bridges was determined directly by TEM of the intact bridge to be 46(8) nm with average density of 105(15) per μm^2 (Song et al. 2003). The corresponding pores seen in the demineralized organic matrix of our samples averaged only half this size, suggesting expansion of the organic matrix into the pore where the mineral bridges were removed. The average pore diameters for *P. maxima* noted above were only 30 nm, and it is likely that the corresponding mineral bridges would be larger, near 60 nm. In that case, the area they occupy could

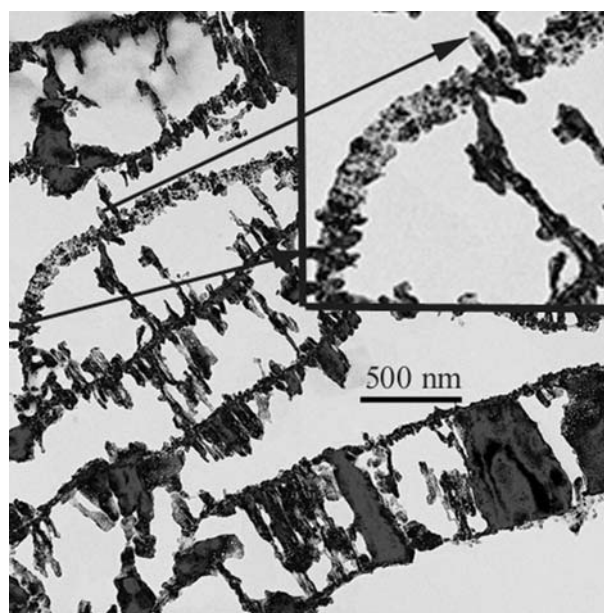


FIGURE 3. TEM micrograph of a whitish pearl showing remnants of the edge-band structure. The widths of the remnants correspond to the band widths shown in Figure 2. A section is shown (inset) enlarged by 2 \times .

increase from 8 to about 16%.

The structure of the tile edge-bands has a growth sense. Our model for the structure of these bands is shown in Figure 6. With reference to the expanded area of Figure 2, the tiles to the right of the gaps are denoted “head” sides; they are formed first and have a sharper onset of the microchannels than those on the adjacent (left-hand) tail side. The edge-bands on adjacent tiles comprise continuous microchannels and extended regions of organic matrix embedded in both sides of the join between tiles. The bands seem to be continuous with and chemically identical or similar to the cementing organic matrix. This organic matrix is described as insoluble (Weiner and Traub 1984) to distinguish it from the water-soluble glycoproteins sometimes also present in the mineral phase (Addadi and Weiner 1985; Miyamoto et al. 1996; Sarashina and Endo 1998). At the onset of band formation, a nearly continuous organic matrix layer forms that extends into a tail-like channel. The channels are 4 nm wide and spaced quite regularly about 12 nm apart. In some places, the aragonite crystal matrix is only 5 to 10 unit cells thick (4 nm) between channels. Based on measurements from Figure 2 and similar images, and assuming a staggered arrangement of channels, we estimate that the organic material is 20% by volume of the tile edge-bands.

It is our contention that the entire double edge-band nanocomposite (edge-band structure extending from each tile, head side and tail side) gives rise to an optical interference film that causes the body color of pearls. In Figure 7 we show the correlation between the first-order Newton’s colors for a film of refractive index of 1.5 and the width of the edge-band structure measured from the beginning of the head side to the finish of the tail side. Table 1 summarizes the data that were obtained from 72 sets of measurements on 7 different pearls covering a range of body colors. In all cases, measurements were made

both of the whole double edge-band structure and of the width of each individual edge-band. The latter was done to control for the effects of tile displacement due to relaxation of the tiles in the thin microtome sections needed to image the bands. However, we were not able to control for possible shrinkage of the gap due to the TEM vacuum. The width of the tile gaps can also depend on the direction of the microtome cut.

We find that the “head” or first grown band is 28(3) nm and

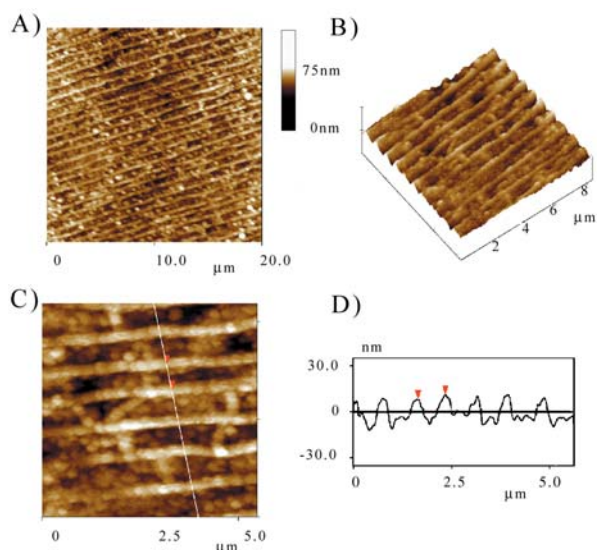


FIGURE 4. The AFM images of a silver pearl. (A) Topographic image (size $20 \times 20 \mu\text{m}$) (B) 3-dimensional image (size $8 \times 8 \mu\text{m}$), (C) Height image (size $5 \times 5 \mu\text{m}$) and (D) corresponding cross section. Figure B shows ridges at the tile junctions and shallow valleys between the ridges over the tile edges.

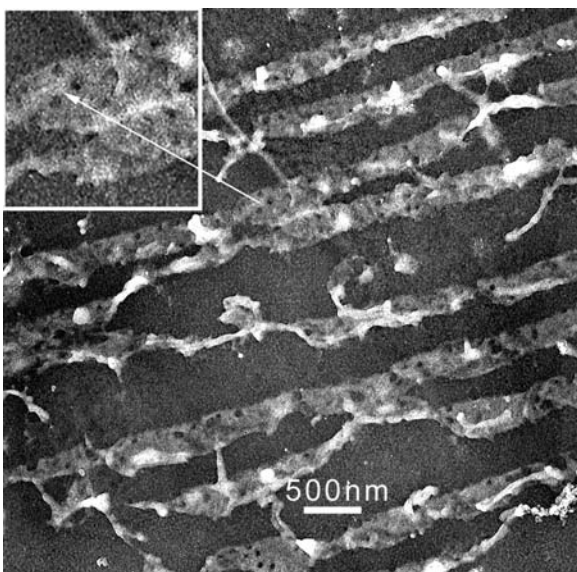


FIGURE 5. Sectioned pearl specimen decalcified and stained by a solution of uranyl acetate ($\text{pH} = 2$) and lead acetate. The stained residual organic matrix binding strips show pores that can accommodate mineral bridges between the aragonite tiles of the nacre. An area (inset) is shown enlarged by 2 \times .

does not change its width significantly with pearl color over the entire group measurements from all 7 pearls examined. This edge-band always starts with a head that is connected to a fine

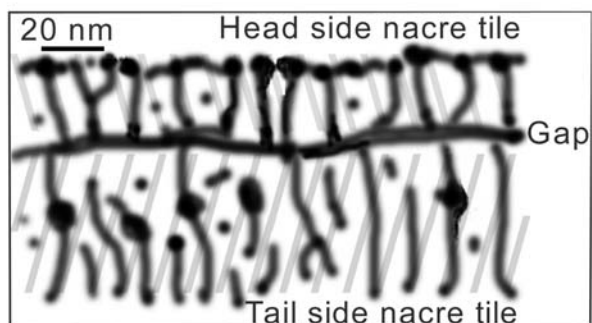


FIGURE 6. Model of the double edge-bands of the nacre tiles shows the difference between the “head” (first grown side), where the onset is marked by an almost continuous line and the “tail” side. All the dark areas represent organic matrix and the diagonal hatching discriminates the adjacent tiles.

TABLE 1. Measured widths (TEM images) of the double edge-band structure and individual edge-bands, nm

	Head side	Tail side	Sum	Double band, Inferred	
				direct Measured	gap
Black	28.6	32.4	61.0		70(4)
Silver	27.7	36.2	63.9	69(4)	4.8
Cream	29.5	43.2	72.7	85(4)	13.8
Gold	28.3	52.5	80.8	90(4)	9.5
Gold lip shell	28.4	52.4	80.8		90(4)
Average	28(3)				9.4

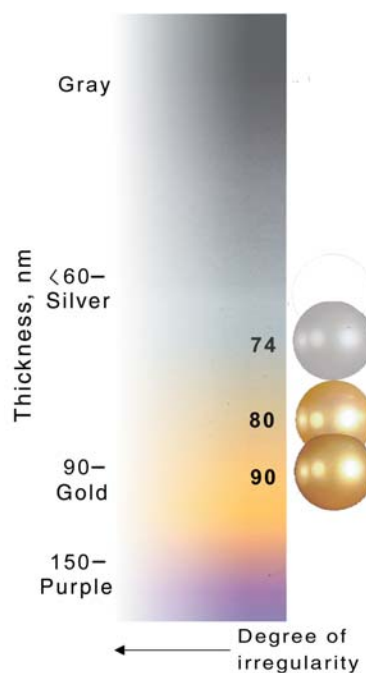


FIGURE 7. Comparison of the Newton’s colors for a film of refractive index 1.5 (extreme right) with the colors of pearls plotted according to their edge-band film thicknesses. The fully saturated colors are shown on the right, but are faded to the left to show the effect of loss of color due to increased irregularity in tiling or edge-band structure.

channel that runs to the edge of the tile. The second band grown on the adjacent tile always terminates in a channel or "tail". By comparing the full-band width to the measured widths of the individual head and tail edge-bands (see Fig. 6), we conclude that the gap between the tiles is between 5 and 14 nm. The total edge-band widths (band indirectly measured) are derived from the individual measurements of the head side, plus the tail side, plus the average gap width of 9.4 nm. The exact value is not as important as the relative widths of the bands in different pearls. The directly and indirectly measured total bands are in good agreement and enable us to get good measures for black pearls and gold lip shell specimens, which could not be otherwise readily obtained due to tile displacement. The edge-band structure thickness ranges from 70(4) to 90(4) nm, a range of 5 standard deviations, and is therefore statistically highly significant.

The *P. margaritifera* pearl (black in Table 1) had an edge-band width structure of 70(4) nm, which is not significantly different from the value for a silver *P. maxima* pearl at 74(4) nm, but the color is a much darker silver. From the Newton color chart (Fig. 7), we would predict an edge-band structure width of 40 to 50 nm for these pearls. These black pearls can be found with very dark colors, and it is likely that a black coloring agent is also present in these pearls (Elen 2002). Both melanin and metalloporphyrins have been cited as the coloring agents (Landman et al. 2001).

DISCUSSION

Optical interference within the aragonite tiles of the nacre is a highly unlikely cause of body color. The average tile thickness is about 400 nm, but can vary widely in the range 300 to 600 nm, and thus would not give rise to a specific interference color. In SEM images of broken pearls, the average thickness of 10 or more tiles show no correlation with pearl color. In contrast, Paua shell, where the aragonite tiles are very regular in thickness and shape, a strong diffraction effect is seen with blue and green colors varying with observation angle. The colors here are further enriched as the tile thickness varies slowly from 250 to 400 nm between growth rings, but they are locally regular (Snow, Pring, and Self unpublished results). These optical diffraction effects (also seen in some feldspars, notably labradorite) are ascribed to the regularity of the layers (Raman 1934), but are not seen in the lip of *P. maxima* shell, where only a single silver, cream, or gold color is seen at all observation angles.

Silver and gold colors, due to interference, are commonly seen in pearly pigments that are formed from mica flakes coated with thin layers of Ti or Fe oxides. The colors arise from out-of-phase interference between light rays scattered from the top and bottom of the coating layers with thicknesses of 60 nm (silver-white) and 105 nm (golden). The color depends on the thickness of the coating material and the refractive index of both the coating material and its environment (Pfaff and Reynders 1999). We contend that the full edge-band structure described above acts as an interference film providing an effective change in refractive index (n) where the structure abuts pure aragonite. Furthermore, we infer that the nacre provides a multi-layer thin-film diffraction layer stack of these bands. For the edge-band structure to act as an interference film, significant scattering with the opposite phase needs to occur at the extreme walls of the double edge-band structure, uninterrupted by the central gap between the

tiles. Changes in n occur at the top of the edge-band structure, at each wall of the central gap between the tiles, and at the bottom of the edge-band structure. The top and bottom of the central gap are separated by only 9 nm and out-of-phase scattering from these points will self cancel (see Fig. 7, dark region). Hence, we are left with the scattering from the limits of the edge-band structure.

The reflectivity, R , of the junctions depends on the refractive index of the materials (denoted by o and i) according to Equation 1 derived by Pfaff and Reynders (1999):

$$R = \{(n_i^2 - n_o^2)/(n_i^2 + n_o^2)\}^2 \quad (1)$$

These authors also provided a method of computing the effective n for a porous or composite medium, which can be used with this expression. Where the pores are filled by a material (denoted o) to a decimal fraction F in the bulk material (denoted a), the effective refractive index n_{eff} can be found from Equation 2:

$$(n_{\text{eff}}^2 - 1)/(n_{\text{eff}}^2 + 2) = (1 - F)(n_a^2 - 1)/(n_a^2 + 2) + F(n_o^2 - 1)/(n_o^2 + 2) \quad (2)$$

Along the [001] direction of aragonite $n=1.53$, and n is close to 1.68 in both the other two axial directions (Battey and Pring 1997). The organic matrix is known to be mainly β -chitin with a lesser amount of glycoprotein (Levi-Kalisman et al. 2001). The most recent measured value of n available for β -chitin is 1.435 (De Cavalho and Vidal 1996) and a value of 1.4 was fitted to data for silverfish (Large et al. 2001). The average refractive index of the edge-band will depend on the volume of aragonite displaced by organic material. If n is taken as 1.435 for β -chitin occupying 20% by volume in the edge-band, the n_{eff} values are 1.51 or 1.627 depending on the crystallographic orientation of the aragonite. The n_{eff} values differ from the n values of aragonite by at least 0.02 and up to 0.05 units corresponding to reflectivities of 0.02 and 0.1% at a single interface. Pfaff and Reynders (1999) stated that a contrast in the value of n should be more than 0.06 for a strong interference effect in multi-layer systems as we have here. However, iridescent organic pigments with contrasts in the range 0.06 to 0.1 show stronger effects than pearls, as the strength of the effect is proportional to the square of the difference of the squares of the component refractive indices (see Eq. 1). Thus, our calculated values in the range 0.02 to 0.05 would give a weaker iridescence, consistent with the comparatively subtle effect in pearls. We note that refractive-index contrasts of this magnitude will be achieved in at least some directions through the tiles, as the refractive indices of aragonite will vary with direction between 1.53 and 1.68. In addition, it is known that pearl has the property of being able to diffuse light around its circumference (Raman 1954), presumably by reflection within the tiles. In this way, light will be available from all directions to give rise to effective interference.

Small changes in the edge-band structure widths can account for the very wide range of pearl color tones seen in *P. maxima* pearls. The strength of the interference effect will depend not only on the spread and average of the edge-band widths but also on the relative size, orientation, and shapes of the individual tiles. This tiling regularity will affect both the intensity and color tone of the pearl or shell. Figure 7 illustrates, in a semi-quantitative

way, how the colors may change as irregularity of the tiling increases. At the limit of the irregularity (far left), the color is totally bleached, but at intermediate points similar colors arise from differing combinations of irregularity in edge-band width and tiling. This model explains the very great range of subtle variations in the color and tone exhibited by pearls. Many pearl oysters produce white or nearly white pearls. Indeed, pearls that have either poorly defined edge-bands or irregular tiling will appear whiter and reflect all wavelengths with less selectivity. The inner nacreous layer of *P. maxima* shell meets this condition; TEM images reveal nacre tiles that are less regular in shape and size than in the outer nacreous layer. An edge band structure exists, but it is poorly defined. Where a pigment is also present in the organic matrix, as in *P. margaritifera* pearls, yet another variable is available for color variations.

Good pearls are afforded by relatively few mollusc species, and the ones that do give attractive pearls, all have shells with strong texture (close alignment of the c axis of the aragonite plates). *P. margaritifera* has the strongest textural alignment reported and the width at half maximum in the distribution of the c-axis texture is 5° (Chateigner et al. 2000). Together with *P. maxima*, *Pinna nobilis*, and *Pteria penguin*, these are the four strongest-textured shells that form sheet nacre. For the formation of pearls colored by thin-film interference, as described above, a strong texture is a precondition to maintain the alignment of the edge-bands.

We are aware of the existence of rose gold pearls (Taylor 2002, personal communication) and predict, because red is next in the Newton's color sequence, that the thickness of the edge-band would be in the range 130 to 150 nm. In pearl-farming operations, experiments directed at obtaining high yields of gold pearls, without the less-desirable cream colors, have proven difficult (Taylor 2002). This difficulty would be explained at least in part by the narrower size range of the edge-band structure width that would give rise to the pure gold color in pearls as compared to wide size range for variously colored silver pearls (see Fig. 7).

ACKNOWLEDGMENTS

We are grateful to Joseph Taylor of Atlas Pacific Limited, (a pearl farmer in Indonesia) for useful discussions and to Atlas Pacific Limited for supplying specimens and a grant in support of this work. We are also grateful to Steve Arrow of Arrow Pearls Pty. Ltd. for discussions and making available copies of the Theses of B.J.A. Vance and of G. Lambert. Shapter and Losic would like to acknowledge the Flinders Institute of Research in Science and Technology (FIRST) for on-going funding and the Australian Research Council (ARC) for infrastructure funding. We are also very grateful for the input of the referees and the sub-editorial help of Jill Pasteris in improving the content and readability of this paper.

REFERENCES CITED

- Addadi, L. and Weiner, S. (1985) Interactions between acidic proteins and crystals: stereochemical requirements in biomineralization. *Proceedings of the National Academy of Science*, 82, 4110–4114.
- Addadi, L. and Weiner, S. (1997) A pavement of pearl. *Nature*, 389, 912–915.
- Akamatsu, S., Komatsu, H., Koizumi, C., and Nonaka, J.A. (1977) Comparison of sugar compositions of yellow and white pearls. *Bulletin of the Japanese Society of Scientific Fisheries*, 43, 773–777.
- Bathey, M.H. and Pring, A. (1997) *Mineralogy for students*, 3rd ed., p. 231. Longman, London.
- Chateigner, D., Hedegaard, C. and Wenk, H.-R. (2000) Mollusc shell microstructures and crystallographic textures. *Journal of Structural Geology*, 22, 1723–1735.
- De Cavalho, H.F. and Vidal, B.D. (1996) Polarised microscopy of an internal sensillum of *Triatoma infestans*: An ordered distribution of chitin fibrils and associated components. *Comptes Rendus de L'Academie des Science, serie III—Sciences de la Vie—Life Sciences*, 319, 33–38.
- Elen, S. (2001) Spectral reflectance and fluorescence characteristics of natural-color and heat-treated "golden" South Seas cultured pearls. *Gems and Gemology*, 37, 114–123.
- (2002) Identification of yellow cultured pearls from the black-lipped oyster *Pinctada Margaritifera*. *Gems and Gemology*, 38, 66–72.
- Frémy, E. (1855) Recherches chimiques sur les os. *Annales de Chimie et Physique* T. 43, 96.
- Glausch, R., Kieser, M., Maisch, R., and Pfaff, G. (1998) *Special Effect Pigments*, Vincentz, Hannover.
- Iwata, K. (1975) Ultrastructure of the conchiolin matrices in molluscan nacreous layer. *Journal of the Faculty of Science, Hokkaido University, Series IV*, 17, 173–229.
- Koizumi, C. and Nonaka, J. (1970) Yellow pigments—II. HCl-methanol soluble yellow pigments. *Bulletin of the Japanese Society of Scientific Fisheries*, 36, 10.
- Lambert, G. (1998) Trace element composition in pearls. Unpublished M.Sc. Thesis, Murdoch University, Western Australia.
- Landman, N.H., Mikkelsen, P.M., Bieler, R., and Bronson, B. (2001) Pearls, a natural history, p. 32–54. American Museum of Natural History and Harry N. Abrams, Inc., New York.
- Large, M.C.J., McKemzie, D.R., Parker A.R., Steel B.C., Ho, K., Bosi, S.G., Nicorovic, N., and McPhedran, R.C. (2001) The mechanism of light reflection in silverfish. *Proceedings of the Royal Society of London, A* 457, 511–518.
- Liu, Y., Shigley, J.E., and Hurwit, K.N. (1999) Iridescence color of a shell of the mollusk *P. Margaritifera* caused by diffraction. *Optics Express*, 4, 177–182.
- Liu, Y., Hurwit, K.N., and Tian, L. (2003) Relationship between the groove density of the grating structure and the strength of iridescence in mollusc shells. *Australian Gemmologist*, 21, 405–407.
- Levi-Kalisman, Y., Falini, G., Addadi, L., and Weiner, S. (2001) Structure of the nacreous organic matrix of a bivalve mollusk shell examined in the hydrated state using cryo-TEM. *Journal of Structural Biology*, 135, 8–17.
- Miyamoto, H., Miyashita, T., Okushima, M., Nakano, S., and Matsushiro, A. (1996) A carbonic anhydrase from the nacreous layer in oyster pearls. *Proceedings of the National Academy of Science*, 93, 9657–9660.
- Nagata, N., Dobashi, T., Manabe, Y., Usami, T., and Inokuchi, S. (1997) Modelling and Visualisation of a pearl quality simulator. *IEEE Transactions on Visualization and Computer Graphics*, 3, 307.
- Newman, R. (1999) *Pearl Buying Guide*, 3rd edition, International Jewellery Publications, Los Angeles.
- Pfaff, G. and Reynders, P. (1999) Angle-dependent optical effects deriving from sub-micron structures of films and pigments. *Chemical Review* 99, 1963–1981.
- Raman, C.V. (1934), On iridescent shells—Part II. Colours of laminar diffraction. *Proceedings of the Indian Academy of Science*, A1, 574–589.
- (1954) The structure and optical behavior of pearls. *Proceedings of the Indian Academy of Science*, A39, 215–222.
- Sarashina, I. and Endo, K. (1998) Primary structure of a soluble matrix protein of scallop shell: Implications for calcium carbonate biomineralization. *American Mineralogist*, 83, 1510–1515.
- Schäffer, T.E., Ionescu-Zanetti, C., Proksch, R., Fritz, M., Walters, D.A., Almqvist, N., Zarembo, M., Belcher, A.M., Smith, B.L., Stuky, G.D., Morse, D.E., and Hansma, P.K., (1997) Does abalone nacre form by heteroepitaxial nucleation or by growth through mineral bridges? *Chemical Materials*, 9, 1731–1740.
- Song, F., Soh, A.K., and Bai, Y.L. (2003) Structural and mechanical properties of the organic matrix layers of nacre. *Biomaterials*, 24, 3623–3631.
- Taylor, J.D., Kennedy, W.J., and Hall, A. (1973) The shell structure and mineralogy of the Bivalvia. *Lucinacea—Clavagellacea. Conclusions. Bulletin of the British Museum of Natural History, Zoology*, 22, 253–294.
- Taylor, J.U. (2002) Producing golden and silver south sea pearls from Indonesian hatchery reared *P. Maxima*, WAS Conference Abstracts, Beijing, China, April 2002.
- Vance, B.J.A. (1995) *Shell Organics Matrices in some Pearl Oysters and other Bivalves*, Unpublished Ph.D. Thesis, James Cook University of North Queensland.
- Wang, R.Z., Suo, Z., Evans, A.G., Yao, N., and Aksay, I.A. (2001) Deformation mechanisms in nacre. *Journal of Materials Research*, 16, 2485–2493.
- Webster, R. and Anderson, B.W. (1983) *Gems, their sources, descriptions and identification*, p. 505–506. Butterworths, London.
- Weiner, S. and Hood, L. (1975) Soluble protein of the organic matrix of mollusk shells: A potential template for shell formation. *Science*, 190, 987–989.
- Weiner, S. and Traub, W. (1984) Macromolecules in mollusc shells and their functions in biomineralization. *Philosophical Transactions of the Royal Society of London*, B304, 425–434.
- Weiner, S., Talmon, Y., and Traube W. (1983) Electron diffraction of mollusc shell organic matrices and their relationship to the mineral phase. *International Journal of the Biology of Macromolecules*, 5, 325–328.

MANUSCRIPT RECEIVED JUNE 6, 2003

MANUSCRIPT ACCEPTED MARCH 10, 2004

MANUSCRIPT HANDLED BY JILL PASTERIS